Journal of Materials Chemistry A

Accepted Manuscript

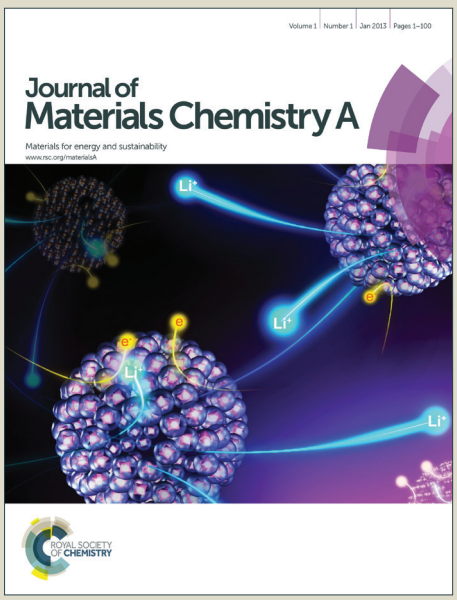

ROYAL SOCIETY OF CHEMISTRY

www.rsc.org/materialsA

Journal of

Materials Chemistry A

PAPER

$Na_{3.12}Fe_{2.44}(P_2O_7)_2$/multi-walled carbon nanotube composite as a cathode material for sodium-ion batteries

Received 00th January 20xx,
Accepted 00th January 20xx

DOI: 10.1039/x0xx00000x

www.rsc.org/

Yubin Niu[1,2], Maowen Xu[1,2,*], Chuanjun Cheng[1,2], ShuJuan Bao[1,2], Junke Hou[1,2], Sangui Liu[1,2], Fenglian Yi[1,2], Hong He[1], Chang Ming Li[1,2,*]

$Na_{3.12}Fe_{2.44}(P_2O_7)_2$/multi-walled carbon nanotube (MWCNT) was fabricated by a solid state reaction and was further used to fabricate a cathode for sodium-ion batteries. The electrochemical behaviors were thoroughly investigated in assembled non-aqueous $Na_{3.12}Fe_{2.44}(P_2O_7)_2$/MWCNT//Na cells, showing higher specific capacity (over 100 mA h g^{-1} at a rate of 0.15C) and better stable cycle performance than that of pristine $Na_{3.12}Fe_{2.44}(P_2O_7)_2$-based one. It is noted that with increased charge-discharge cycles, the specific capacity of $Na_{3.12}Fe_{2.44}(P_2O_7)_2$/MWCNT is getting close to the theoretical capacity (ca. 117.4 mA h g^{-1}). These good performances could be attributed to the incorporated MWCNTs, which improve the conductivity for lower charge transfer resistance and shorten diffusion length for faster Na^+ diffusion to access the reaction sites. Through systematic studies of EIS at different states of charge and discharge, it is discovered that R_{ct} decreases with the increase of voltage and reachs a minimum value at redox sites, but R_e and D_{Na^+} go to the opposite. Moreover, a full cell test using a carbon black negative electrode also demonstrates good capacity retention up to 50 cycles and a reversible capacity of 145 mAh g^{-1} with the average operation voltage of 2.8 V.

Introduction

Nowadays, lithium ion batteries (LIBs) which have the highest energy density are successfully used in energy storage power stations, hybrid electrical vehicles (HEVs) and electrical vehicles (EVs), but its further application is limited by disadvantages such as high cost and scarce resource of lithium. Therefore, the employment of other guest ion as an alternative to lithium-ion is favorable to further development of the intercalation chemistry. As a member in post-lithium ion batteries, sodium-ion batteries (NIBs) have been gaining increasing attention thanks to the natural abundance, low cost, low toxicity and similar to LIBs in electrochemical reaction mechanism. However, the higher redox potential (-2.71V *vs.* SHE) of Na/Na^+ lowers the cell voltage of NIBs, whilst the larger ionic radius (1.02 Å) of Na^+ and orbital sizes make it more difficult to find a suitable host for sodium ion de/intercalation.[1-3]

To date, numerous kinds of intercalation hosts have been studied for Na ions. Various layered oxides, such as Na_xMO_2 (M=Mn, Fe, Co, Ni)[1, 2, 4-6], $Na_xFe_{0.5}Mn_{0.5}O_2$[7, 8], $NaNi_{0.5}Mn_{0.5}O_2$[9], $NaNi_{0.25}Fe_{0.5}Mn_{0.25}O_2$[10], $Na_{0.67}Mn_{0.65}Fe_{0.2}Ni_{0.15}O_2$[11], $Na_{0.70}Mn_{0.60}Ni_{0.30}Co_{0.10}O_2$[12], $Na_{0.67}Mn_{0.65}Co_{0.2}Ni_{0.15}O_2$[13], $Na_{2/3}Ni_{1/3}Mn_{2/3-x}Ti_xO_2$[14], and $Na_xLi_yNi_zMn_{1-y-z}O_2$ ($0 < x, y, z < 1$)[15] are performed to sodium intercalation. However, their unsatisfactory long term stability of host structure, low operating voltage and high polarization prohibit their practical application. In stark contrast to the layered oxide, the sodium containing polyanion and mixpolyanion compounds have more stable host frameworks, which result in their longer cycle life and better safety[3], and allow the monitoring of given $M^{n+}/M^{(n-1)+}$ redox couple, through the inductive effect[16].

Recently, various phosphorus-based polyanion materials such as $Na_3V_2(PO_4)_3$[17-22], $NaFePO_4$[23], $Na_2FeP_2O_7$[24], $Na_2MnP_2O_7$[25], $Na_3M_2(PO_4)_2F_3$ (M = Ti, Fe, V)[26], $Na_7V_4(P_2O_7)_4(PO_4)$[3, 27], $Na_2Fe_{3-x}Mn_x(PO_4)_3$[28], $Na_4Fe_3(PO_4)_2(P_2O_7)$[29] and $Na_{4-\alpha}M_{2+\alpha/2}(P_2O_7)_2$ ($2/3 \leq \alpha \leqslant 7/8$, M = Fe, $Fe_{0.5}Mn_{0.5}$, Mn)[30] were reported. Of them, $Na_{3.12}Fe_{2.44}(P_2O_7)_2$ as a new polyanion-based cathode materials was only been reported by one paper[30]. The voltage electrode demonstrate that a reversible capacity of 85 mA h g^{-1} (1.76 Na) with stable cycle performance at a rate of ca. 0.04C (4.8 mA g^{-1}). The theoretical capacity of $Na_{3.12}Fe_{2.44}(P_2O_7)_2$ is 117.4 mA h g^{-1}, assuming that 2.44 Na is reversibly de/intercalated by means of oxidation and reduction of 2.44 Fe^{2+}/Fe^{3+}. That is to

[a] *Institute for Clean Energy & Advanced Materials, Faculty of Materials and Energy , Southwest University, Chongqing 400715, P.R. China.*
[b] *Chongqing Key Laboratory for Advanced Materials and Technologies of Clean Energies, Chongqing 400715, P.R. China.*
* Corresponding author
E-mail: ecmli@swu.edu.cn or xumaowen@swu.edu.cn
Electronic Supplementary Information (ESI) available: [details of any supplementary information available should be included here]. See DOI: 10.1039/x0xx00000x

say, there could be further to go for the capacity. Considering a disadvantage of polyanion cathode materials is poor conductivity, the key to solve the problem is to improve the electrical conductivity of the material. Herein, we report that expanded MWCNTs adhesive $Na_{3.12}Fe_{2.44}(P_2O_7)_2$, which was synthesized by carbonization mechanism of sucrose, results in excellent electrochemical properties in both half-cell of NIBs and full cell using carbon black as negative electrode.

Experimental section

All chemical reagents were analytical grade and were used as received.

Synthesis

$Na_{3.12}Fe_{2.44}(P_2O_7)_2$ powders were synthesized by a solid state reaction. Na_2CO_3, $FeC_2O_4{\cdot}2H_2O$, and $(NH_4)_2HPO_4$ were wet ball-milled with ethanol as solvent in a stoichiometric molar ratio. The powders were heated at 450 °C for 6 h under an Ar atmosphere, and then at 600 °C for 12 h under an Ar atmosphere. The sample $Na_{3.12}Fe_{2.44}(P_2O_7)_2$/MWCNT was prepared following the same experimental conditions but adding amount of MWCNT (5 wt%) and sucrose (5 wt%).

Materials characterization

Powder X-ray diffraction (XRD, MAXima-X XRD-7000) using Cu Kα radiation was employed to identify the crystalline phase of the material. The experiment was performed by using step mode with a fixed time of 1 s and a step size of 0.02°. The morphology and microstructure were examined by field-emission scanning electron microscopy (SEM, JSM-6700F) and transmission electron microscopy (TEM, JEM-2100). Thermogravimetric analysis (TGA, Q50) was carried out in flowing air. The precursor was heated from 30 to 800 °C at a rate of 5 °C min^{-1}. The carbon content in the $Na_{3.12}Fe_{2.44}(P_2O_7)_2$/MWCNT composite was determined by acid soluble weight difference method.

Electrochemical measurements

Coin cells were assembled to carry out the electrochemical measurements. The composite electrode was made from a mixture of the prepared sample, carbon black, and polyvinylidene fluoride in a weight ratio of 70:15:15. A disk of sodium foil was used as counter electrode and 1 $mol{\cdot}L^{-1}$ $NaClO_4$ dissolved in a mixture of ethylene carbonate (EC) - diethyl carbonate (DEC) was used as electrolyte. For the galvanostatic intermittent titration technique (GITT), a constant current of 0.05 C was applied for 10 min, and then, it was interrupted to achieve the open circuit condition for 40 min. This process was repeated until the electrode potential reached the cutoff voltage. Galvanostatic charge-discharge tests were performed in the potential range of 1.7~4.0 V vs Na/Na^+ at ambient temperature on a Land battery testing system (Wuhan, China). All the specific capacities are calculated on the basis of $Na_{3.12}Fe_{2.44}(P_2O_7)_2$ only. Cyclic voltammogram (CV) was measured at a scan rate of 0.05 mV s^{-1} between 1.7 and 4.0 V using an Arbin Instruments testing system. Electrochemical impedance spectroscopy (EIS) experiments were conducted in the frequency range of 0.01-100 kHz with a CHI600D electrochemical analyzer.

Results and discussion

$Na_{3.12}Fe_{2.44}(P_2O_7)_2$ crystallizes in a triclinic structure (space group: *P-1*). Fig. 1a (along a- and b-axis) schematically shows that the framework of $Na_{3.12}Fe_{2.44}(P_2O_7)_2$ is built on a centrosymmetrical crown of $Fe_2P_4O_{22}$ and $Fe_2P_4O_{20}$ moitiés connected by corner-sharing to form a three-dimensional framework. Each crown unit consists of two FeO_6 octahedra and two P_2O_7 groups. Figure 1b shows two kinds of products of XRD patterns; the similar XRD patterns could be well indexed to tricline $Na_{3.12}Fe_{2.44}(P_2O_7)_2$ structure, which is consistent with the literature[30]. This suggests that the crystal structures of $Na_{3.12}Fe_{2.44}(P_2O_7)_2$ are independent of the employed carbon source in synthesis. In addition, it also can be seen that the crystallization degree of the composite is better than non-composite, especially the two peaks between 16° and 18° were obvious.

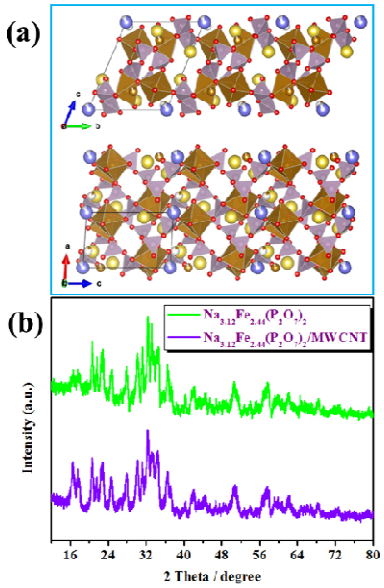

Fig. 1. (a) Crystal structure model of triclinic $Na_{3.12}Fe_{2.44}(P_2O_7)_2$ and $Na_{3.12}Fe_{2.44}(P_2O_7)_2$/MWCNT, (b) XRD pattern of as-prepared $Na_{3.12}Fe_{2.44}(P_2O_7)_2$ materials.

Fig. 2 shows the formation mechanism of as-prepared products based on thermogravimetric (TG) analysis. Both precursors have similar decomposition trends, except the product formation temperature of $Na_{3.12}Fe_{2.44}(P_2O_7)_2$/MWCNT reduced from 535 ℃ to 450 ℃. This is because the carbonation process of sucrose is exothermic reaction, the heat released provides energy for the products formation. Based on this knowledge, we can use the method of pyro-synthesis to get many functional materials[31]. In addition, under the same reaction temperature and time, formation temperature decreased to some extent improved the crystallinity of product, which is consistent with the results of XRD patterns.

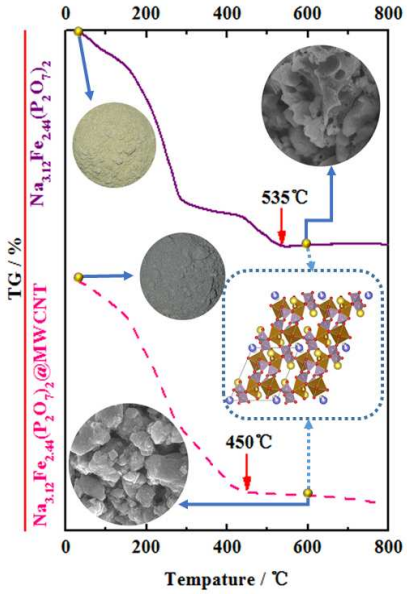

Fig. 2. Formation mechanism of as-prepared products based on thermogravimetric (TG) analysis.

From Fig. 3a and c we can see the surface of $Na_{3.12}Fe_{2.44}(P_2O_7)_2$/MWCNT more rough than that of $Na_{3.12}Fe_{2.44}(P_2O_7)_2$. By the high magnification images (Fig. 3d), we can clearly see MWCNTs adhere to the surface of the active materials. This adhesion effect was attributed to melting and carbonization of sucrose. That is to say, in the synthesis process, with the increase of temperature, sucrose has played the role of "glue" by continuously melting and adhering to the precursors´ particle and MWCNTs surface; when reaching the carbonization temperature, active substance and MWCNTs were firmly nailed together by the carbonization products of sucrose. Furthermore, the obtained products´ primary particle size is approximately 100 nm.

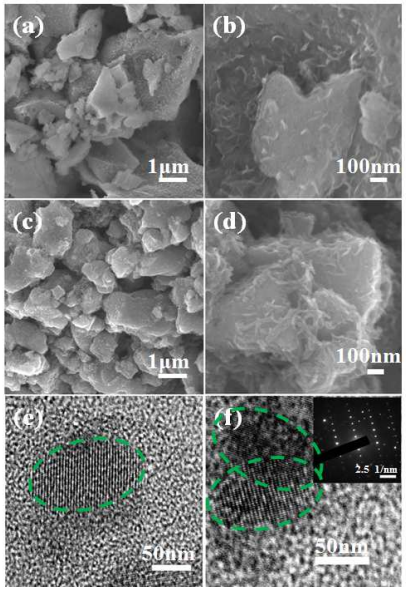

Fig. 3. SEM images of $Na_{3.12}Fe_{2.44}(P_2O_7)_2$ (a and b) and $Na_{3.12}Fe_{2.44}(P_2O_7)_2$/MWCNT (c and d), high-resolution TEM images of $Na_{3.12}Fe_{2.44}(P_2O_7)_2$/MWCNT (the inset shows the selected area electron diffraction) (e and f).

In order to compare the electrochemical performance of two kinds of materials, the samples were assembled to coin cells. The cycle performance of $Na_{3.12}Fe_{2.44}(P_2O_7)_2$ and $Na_{3.12}Fe_{2.44}(P_2O_7)_2$/MWCNT were carried out at the rate of 0.04C and 0.15C, respectively, as shown in Fig. 4a. Although the current density of $Na_{3.12}Fe_{2.44}(P_2O_7)_2$/MWCNT is more higher (ca. 4 times) than that in $Na_{3.12}Fe_{2.44}(P_2O_7)_2$, the former still has high specific capacity and cycling stability, and with the cycles increasing, the specific capacity of $Na_{3.12}Fe_{2.44}(P_2O_7)_2$/MWCNT is close to the theoretical capacity. Fig. S1 compares the discharge rates of $Na_{3.12}Fe_{2.44}(P_2O_7)_2$/MWCNT with those of $Na_{3.12}Fe_{2.44}(P_2O_7)_2$, indicating that the former exhibits higher specific capacities and better rate performance. In detail, the former cathode has rate performance of reversible discharge capacity as 104.6 mA h g^{-1} at 0.04C, 86.3 mA h g^{-1} at 0.2 C, 67.2 mA h g^{-1} at 0.5 C, 51.2 mA h g^{-1} at 1.0C and 40.1 mA h g^{-1} at 1.5 C, respectively, while the latter electrode can only deliver discharge specific capacities of 87.1, 62.1, 43.8, 33.4 and 23.1 mA h g^{-1} at 0.04, 0.2, 0.5, 1.0 and 1.5 C, respectively. Moreover, the reversible discharge capacity of the former cathode can retain to 62.3 mA h g^{-1} when the discharge rate changes back to 0.5 C after 36 cycles, demonstrating that the cathode is tolerant to varied discharge current and the capacity can even recover to the original value as long as the current reverses back to the low rates. From the Nyquist diagrams, as shown in Fig. 4b, we can see that the $Na_{3.12}Fe_{2.44}(P_2O_7)_2$/MWCNT has lower electrochemical impedance. Moreover, the chemical diffusion coefficient of Na^+ (D_{Na^+}) could be calculated according to the following equation [Eq. (1)]:

$$D_{Na^+} = \left(\frac{2RT}{\sqrt{2}n^2F^2\sigma_W AC}\right)^2 = \frac{2R^2T^2}{n^4F^4\sigma_W^2A^2C^2}$$

where R, T, A, F, n and C are the gas constant, the absolute temperature, the surface area of the electrode ($Na_{3.12}Fe_{2.44}(P_2O_7)_2$:11.207$m^2$ g^{-1}; $Na_{3.12}Fe_{2.44}(P_2O_7)_2$/MWCNT:21.364 m^2 g^{-1}), the Faraday´s constant, the number of electrons per molecule during oxidation, the Na^+ concentration in the cathode material, respectively. σ_W is the Warburg coefficient which has relationship with Z´ as follows [Eq. (2)]:

where R_s and R_{ct} represent the solution resistance and the charge transfer resistance, respectively.

Fig. 4b (inset image) represents the reciprocal square root of angular frequency ($\omega^{-1/2}$) dependence of the real impedance (Z´) in the low frequency of $Na_{3.12}Fe_{2.44}(P_2O_7)_2$ and

$Na_{3.12}Fe_{2.44}(P_2O_7)_2$/MWCNT. Based on the linear plot slope of Z´ *vs*. $\omega^{-1/2}$, it is found that the estimated sodium diffusion coefficient of $Na_{3.12}Fe_{2.44}(P_2O_7)_2$/MWCNT ($1.02\times10^{-15}$ cm^2 s^{-1}) is higher than $Na_{3.12}Fe_{2.44}(P_2O_7)_2$ (7.95×10^{-16} cm^2 s^{-1}). These results clearly suggest that the kinetics of $Na_{3.12}Fe_{2.44}(P_2O_7)_2$ can be improved by mixing MWCNTs. Conductivity of electrode materials has a crucial influence on its performance[32] and an efficient conductive network and its connections to active material particles are equally critical to ensuring good electrode performance[33]. The intrinsically flexible MWCNTs could buffer stress and strain upon Na^+ ion extraction/reinsertion, and thus retain the connection of particles to the conductive network[34, 35]. This explains why the cycle stability and capacity performance of $Na_{3.12}Fe_{2.44}(P_2O_7)_2$/MWCNT is better than those of $Na_{3.12}Fe_{2.44}(P_2O_7)_2$.

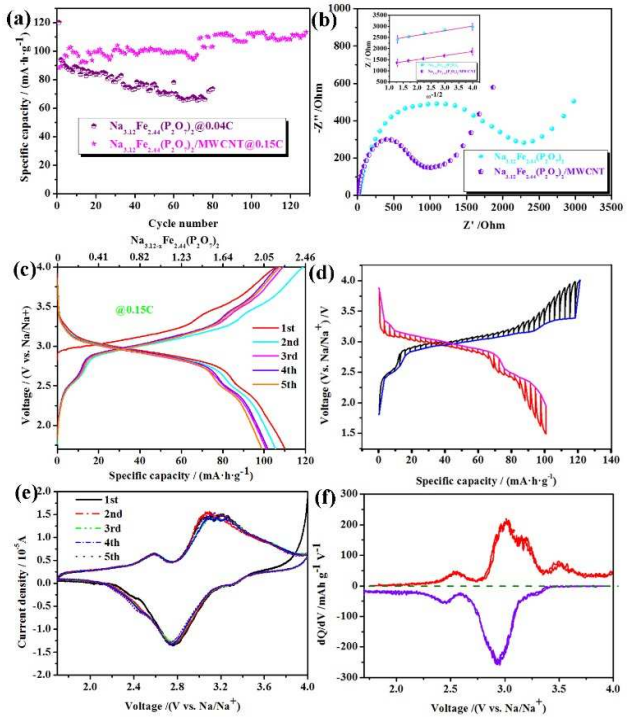

Fig. 4. Cycle performance (a) and EIS (the inset shows Z´ *vs.* $\omega^{-1/2}$ plots in the low frequency) after 3 cycles (b) of $Na_{3.12}Fe_{2.44}(P_2O_7)_2$ and $Na_{3.12}Fe_{2.44}(P_2O_7)_2$/MWCNT; The first five cycles´ voltage profiles at 0.15C (c), GITT evaluation (d), cyclic voltammogram plots before cycles against the Na electrode at a scan rate of 0.05 mV/s (e) and the differential capacity *vs* voltage (dQ/dV) curves calculated from (c) (f) of $Na_{3.12}Fe_{2.44}(P_2O_7)_2$/MWCNT.

GITT measurement and voltage profiles were employed to clarify the nature of sodium de/intercalation (Fig. 4c and d). The voltage profiles of the $Na_{3.12}Fe_{2.44}(P_2O_7)_2$ active materials demonstrate that a reversible capacity of over 100 mA h g^{-1} (ca. 2 Na) is delivered at the rate of 0.15C. Both the charge and discharge curves have three major potential plateaus, and the reactions in the process of sodium extraction can be described by the following three equations [Eq. (3) ~ (5)]:

These results are consistent with those reported by Ha et al., who attribute the $Na_{3.12}Fe_{2.44}(P_2O_7)_2$ electrode proceeds in a one-phase reaction[30]. In order to more clearly demonstrate the existence of plateaus, we conducted cyclic voltammetry (CV) studies and got the differential capacity (d*Q*/d*V*) *vs* voltage curve (Fig. 4 and f). The obtained curves by the above two methods have the same number of peaks, but the latter is more obvious. The oxidation/reduction peaks in Fig. 4 e and f correspond to the charge/discharge plateaus in Fig. 4 c and d. As shown in Fig. 4 e and f, each oxidation peak is paired with a reduction peak. The 2.56V/2.45V pair can be attributed to the phase transition between

and

whose equilibrium potential is 2.51V, the 3.02V, 3.18V/2.94V pair can be attributed to the phase transition between

and

whose equilibrium potential is 3.02V, while the 3.49V/3.33V pair can be attributed to the phase transition between

and

whose equilibrium potential is 3.41V. Although the voltage plateaus of $Na_{3.12}Fe_{2.44}(P_2O_7)_2$ active materials is not very high, we believe that this weakness will be overcome by modification, and which is currently under further investigation in our lab.

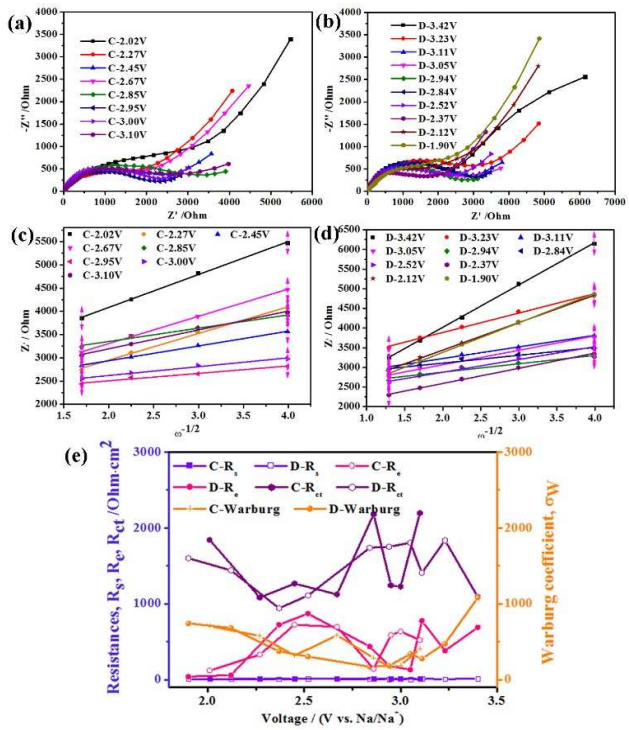

Fig. 5 Nyquist plots of as-prepared materials at different states of charge (a) and discharge (b), respectively; the corresponding plots of the real part of impedance (Z') as a function of the inverse square root of the angular frequency ($\omega^{-1/2}$) at different voltages in the Warburg region (c), (d); changes of EIS parameters values (the solution resistance R_s, the diffusion resistance of Na^+ ions through SEI layer R_e, the charge transfer resistance R_{ct} and Warburg coefficient σ_W) calculated by equivalent circuits and Eq. (2) (f).

Fig. 5 represents Nyquist plots (a, b), the corresponding plots of the real part of impedance as a function of the inverse square root of the angular frequency (c, d) and changes of EIS parameters values calculated by equivalent circuits and Eq. (2) at different states of charge and discharge (f), respectively. For a completely charge and discharge cycle, whether it is the charge or discharge, the change trend of the corresponding parameters are basically the same, that is, R_s remain stable whether at different depth of charge or discharge; R_e increases gradually with the increase of voltage, up to the maximum at 2.5V, then gradually decreased and slightly increased at about 3.0V. On the contrary, R_{ct} decreases with the increase of voltage, reaches a minimum value at 2.5V, then gradually increased and slightly reduced at about 3.0V. In addition, σ_W and D_{Na^+} is inversely proportional to the relationship, we can see from Fig. 5f, along with the increase of voltage, σ_W decreases and reaches the minimum value at about 3.0V, that is, D_{Na^+} increased gradually and reached the maximum value at about 3.0V. From the preceding analysis (Fig. 4) we can know that there are two mainly pair of the oxidation/reduction peaks at 2.5V and 3.0V, the redox sites have the highest reaction activity, so after few cycles, battery activated and SEI film thickness and pores are basically in the stable state. As the voltage increase, the reaction activity gradually increased, R_{ct} reduced, resulting in D_{Na^+} and the number of sodium ions passing through SEI film with a certain number of pores increases, channel become crowded, which leads to the increase of R_e.

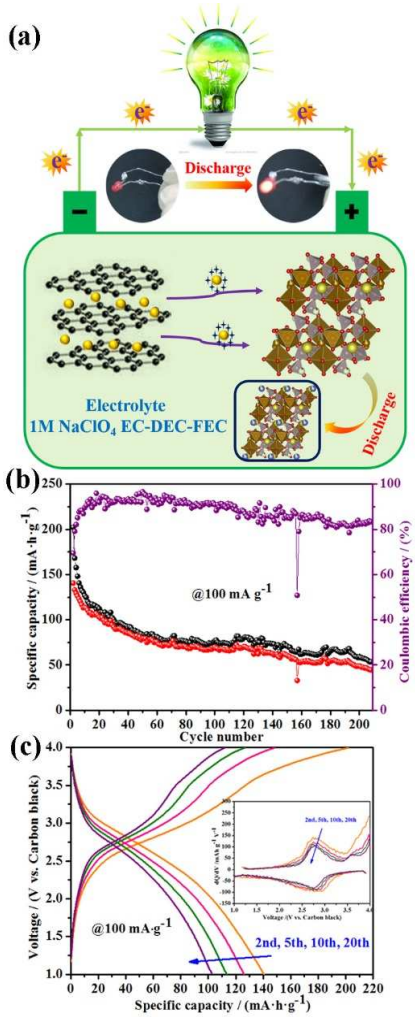

Fig. 6 The Na storage performance of a $Na_{3.12}Fe_{2.44}(P_2O_7)_2$/MWCNT//carbon black full cell cycled at 100 mA g^{-1}. (a) Schematic drawing of the $Na_{3.12}Fe_{2.44}(P_2O_7)_2$/MWCNT//carbon black cell during discharge. On the anode side, the sodiated carbon were transformed into carbon black during discharging, and the reverse reaction took place during charging. On the cathode side, Na^+ surrounded by solvent molecules was intercalated and de-intercalated into $Na_{3.12}Fe_{2.44}(P_2O_7)_2$ structure during charge and discharge reactions, respectively; (b) Long-term stability test and (c) charge-discharge curves for the 2nd, 5th, 10th and 20th cycles, respectively (the inset shows the corresponding the differential capacity *vs* voltage curves).

To demonstrate the application prospects of the sample, we constructed a full sodium-ion battery (see diagram in Fig. 6a) with the $Na_{3.12}Fe_{2.44}(P_2O_7)_2$/MWCNT positive electrode and the carbon black negative electrode. The full cell was cycled at 100 mA g^{-1}, and the preliminary results of electrochemical measurement are displayed in Fig. 6b and c. The $Na_{3.12}Fe_{2.44}(P_2O_7)_2$/MWCNT//carbon black full cell delivers a capacity of 145 mAh g^{-1} (based on carbon black negative mass) and a coulombic efficiency of 70%, respectively. The average operation voltage is around 2.8 V. The capacity of full cell has

only 81 mAh g^{-1} after 50 cycles. Hereafter, improving the full cell´s cycle performance and finding suitable negative to match $Na_{3.12}Fe_{2.44}(P_2O_7)_2$/MWCNT are our next focus.

Conclusions

In summary, $Na_{3.12}Fe_{2.44}(P_2O_7)_2$/MWCNT composite was fabricated by a solid state reaction. Results show that the Na-ion battery based on $Na_{3.12}Fe_{2.44}(P_2O_7)_2$/MWCNT cathode materials achieves higher specific capacity and better stable cycle performance, over 130 cycles than that of pristine $Na_{3.12}Fe_{2.44}(P_2O_7)_2$. Through the systematic study of EIS at different states of charge and discharge, it is found that R_{ct} decreases with the increase of voltage but R_e and D_{Na^+} increase. When pairing with carbon black negative electrode for a full cell, a reversible capacity of 145 mAh g^{-1} with the average operation voltage of 2.8 V was achieved, holding a great promise for practical application. It is proposed that the performance enhancement is resulted by the composed MWCNTs, which improve the electric conductivity for faster interfacial charge transfer while reducing the Na^+ diffusion length for faster Na^+ diffusion to access the reaction sites with a higher mass transport.

Acknowledgements

This work is financially supported by Chongqing Key Laboratory for Advanced Materials and Technologies of Clean Energies under cstc2011pt-sy90001, Start-up grant under SWU111071 from Southwest University and Chongqing Science and Technology Commission under cstc2012gjhz90002. The work is also supported by grants from Fundamental Research Funds for the Central Universities (SWU113079, XDJK2014C051) and Program for the Youth Talent in Science and Technology of Ch ongqing(cstc2014kjrc-qnrc50006).

Notes and references

1 J. Billaud, G. Singh, A. R. Armstrong, E. Gonzalo, V. Roddatis, M. Armand, T. Rojo and P. G. Bruce, *Energy Environ. Sci.*, 2014, **7**, 1387-1391.
2 M. H. Han, E. Gonzalo, G. Singh and T. Rojo, *Energy Environ. Sci.*, 2015, **8**, 81-102.
3 C. Deng and S. Zhang, *ACS Appl. Mater. Interfaces*, 2014, **6**, 9111-9117.
4 N. Bucher, S. Hartung, A. Nagasubramanian, Y. L. Cheah, H. E. Hoster and S. Madhavi, *ACS Appl. Mater. Interfaces*, 2014, **6**, 8059-8065.
5 Y. Cao, L. Xiao, W. Wang, D. Choi, Z. Nie, J. Yu, L. V. Saraf, Z. Yang and J. Liu, *Adv. Mater.*, 2011, **23**, 3155-3160.
6 F. Sauvage, L. Laffont, J. M. Tarascon and E. Baudrin, *Inorg. Chem.*, 2007, **46**, 3289-3294.
7 N. Yabuuchi, M. Kajiyama, J. Iwatate, H. Nishikawa, S. Hitomi, R. Okuyama, R. Usui, Y. Yamada and S. Komaba, *Nat. Mater.*, 2012, **11**, 512-517.
8 H. Zhu, K. T. Lee, G. T. Hitz, X. Han, Y. Li, J. Wan, S. Lacey, A. v. W. Cresce, K. Xu, E. Wachsman and L. Hu, *ACS Appl. Mater. Interfaces*, 2014, **6**, 4242-4247.
9 X. Xia and J. R. Dahn, *J. Electrochem. Soc.*, 2012, **159**, A1048-A1051.
10 S.-M. Oh, S.-T. Myung, C. S. Yoon, J. Lu, J. Hassoun, B. Scrosati, K. Amine and Y.-K. Sun, *Nano letters*, 2014, **14**, 1620-1626.
11 D. Yuan, X. Hu, J. Qian, F. Pei, F. Wu, R. Mao, X. Ai, H. Yang and Y. Cao, *Electrochim. Acta*, 2014, **116**, 300-305.
12 J. Yoshida, E. Guerin, M. Arnault, C. Constantin, B. Mortemard de Boisse, D. Carlier, M. Guignard and C. Delmas, *J. Electrochem. Soc.*, 2014, **161**, A1987-A1991.
13 D. Yuan, W. He, F. Pei, F. Wu, Y. Wu, J. Qian, Y. Cao, X. Ai and H. Yang, *J. Mater. Chem. A*, 2013, **1**, 3895-3899.
14 H. Yoshida, N. Yabuuchi, K. Kubota, I. Ikeuchi, A. Garsuch, M. Schulz-Dobrick and S. Komaba, *Chem. Commun.*, 2014, **50**, 3677-3680.
15 J. Xu, D. H. Lee, R. J. Clément, X. Yu, M. Leskes, A. J. Pell, G. Pintacuda, X.-Q. Yang, C. P. Grey and Y. S. Meng, *Chem. Mater.*, 2014, **26**, 1260-1269.
16 C. Masquelier and L. Croguennec, *Chem. Rev.*, 2013, **113**, 6552-6591.
17 Z. Jian, W. Han, X. Lu, H. Yang, Y.-S. Hu, J. Zhou, Z. Zhou, J. Li, W. Chen, D. Chen and L. Chen, *Adv. Energy Mater.*, 2013, **3**, 156-160.
18 Z. Jian, C. Yuan, W. Han, X. Lu, L. Gu, X. Xi, Y.-S. Hu, H. Li, W. Chen, D. Chen, Y. Ikuhara and L. Chen, *Adv. Funct. Mater.*, 2014, **24**, 4265-4272.
19 Z. Jian, L. Zhao, H. Pan, Y.-S. Hu, H. Li, W. Chen and L. Chen, *Electrochem. Comm.*, 2012, **14**, 86-89.
20 Y. H. Jung, C. H. Lim and D. K. Kim, *J. Mater. Chem. A*, 2013, **1**, 11350-11354.
21 S. Kajiyama, J. Kikkawa, J. Hoshino, M. Okubo and E. Hosono, *Chem.-Eur. J.*, 2014, **20**, 12636-12640.
22 J. Kang, S. Baek, V. Mathew, J. Gim, J. Song, H. Park, E. Chae, A. K. Rai and J. Kim, *J. Mater. Chem.*, 2012, **22**, 20857-20860.
23 M. Avdeev, Z. Mohamed, C. D. Ling, J. Lu, M. Tamaru, A. Yamada and P. Barpanda, *Inorg. Chem.*, 2013, **52**, 8685-8693.
24 P. Barpanda, G. Liu, C. D. Ling, M. Tamaru, M. Avdeev, S.-C. Chung, Y. Yamada and A. Yamada, *Chem. Mater.*, 2013, **25**, 3480-3487.
25 P. Barpanda, T. Ye, M. Avdeev, S.-C. Chung and A. Yamada, *J. Mater. Chem. A*, 2013, **1**, 4194-4197.
26 K. Chihara, A. Kitajou, I. D. Gocheva, S. Okada and J.-i. Yamaki, *J. Power Sources*, 2013, **227**, 80-85.
27 C. Deng, S. Zhang and Y. Wu, *Nanoscale*, 2015, **7**, 487-491.
28 W. Huang, B. Li, M. F. Saleem, X. Wu, J. Li, J. Lin, D. Xia, W. Chu and Z. Wu, *Chem.-Eur. J.*, 2014, **21**, 851-860.
29 J. Y. Jang, H. Kim, Y. Lee, K. T. Lee, K. Kang and N.-S. Choi, *Electrochem. Comm.*, 2014, **44**, 74-77.
30 K.-H. Ha, S. H. Woo, D. Mok, N.-S. Choi, Y. Park, S. M. Oh, Y. Kim, J. Kim, J. Lee, L. F. Nazar and K. T. Lee, *Adv. Energy Mater.*, 2013, **3**, 770-776.
31 J. Gim, V. Mathew, J. Lim, J. Song, S. Baek, J. Kang, D. Ahn, S.-J. Song, H. Yoon and J. Kim, *Sci. Rep.*, 2012, **2**, 1-6.
32 J. B. Goodenough and Y. Kim, *Chem. Mater.*, 2010, **22**, 587-603.

33 I. V. Thorat, V. Mathur, J. N. Harb and D. R. Wheeler, *J. Power Sources*, 2006, **162**, 673-678.
34 C. de las Casas and W. Li, *J. Power Sources*, 2012, **208**, 74-85.
35 X.-Y. Liu, H.-J. Peng, Q. Zhang, J.-Q. Huang, X.-F. Liu, L. Wang, X. He, W. Zhu and F. Wei, *ACS Sustain. Chem. Eng.*, 2014, **2**, 200-206.